Nuclear Inst. and Methods in Physics Research, A 908 (2018) 110–116

Contents lists available at ScienceDirect

Nuclear Inst. and Methods in Physics Research, A

journal homepage: www.elsevier.com/locate/nima

Evaluation of Eu:LiCAF for neutron detection utilizing SiPMs and portable electronics

Michael A. Ford [a,*], Buckley E. O'Day [a], John W. McClory [a], Manish K. Sharma [c], Areg Danagoulian [b]

[a] Air Force Institute of Technology, Department of Engineering Physics, 2950 Hobson Way, Wright-Patterson AFB, OH 45433, United States
[b] Massachusetts Institute of Technology, Department of Nuclear Science and Engineering, 77 Massachusetts Ave, Cambridge, MA 02139, United States
[c] University of Michigan, Department of Nuclear Engineering and Radiological Sciences, 2355 Bonisteel Boulevard, Ann Arbor, MI 48109, United States

ARTICLE INFO

Keywords:
Neutron detection
LiCAF
Pulse shape analysis

ABSTRACT

With the increasing cost and decreasing availability of ^{3}He, there have been many efforts to find alternative neutron detection materials. Lithium calcium aluminum fluoride (LiCAF) enriched to 95% ^{6}Li doped with europium was evaluated here as a replacement material for ^{3}He. Wafers 0.5 cm thick, consisting of LiCAF crystals in a rubberized matrix, were embedded with wavelength shifting fibers (WSF) and mated to silicon photo-multipliers (SiPMs) to measure the photon response in a flux of neutrons from a DD neutron generator. Excellent discrimination was realized between neutrons and gammas, and both pulse-height discrimination and pulse-shape analysis were explored. A Figure of Merit (FoM) of 1.03 was achieved. By applying pulse-shape analysis, a simple neutron count output was generated by utilizing a low-pass filter to suppress fast pulses from the SiPM output and subsequently applying a threshold to the remaining signal. Custom electronics were built to bias the SiPMs, then amplify, filter, discriminate, and digitize the LiCAF/WSF scintillation photons, resulting in a digital pulse that can easily be counted with any microcontroller or field programmable gate array. A significant advantage of LiCAF is that it can be fabricated into any shape/size (when embedded in a rubberized matrix), and the light output and transparency is sufficient to allow for thicker scintillators which enable detection of both thermal and epithermal neutrons. This work demonstrated that Eu:LiCAF is capable of discriminating gammas from neutrons and is a potential replacement material for ^{3}He, especially for nuclear security applications and neutron spectroscopy.

1. Introduction

Neutron detection has been investigated for decades, and it has been an enduring goal of the nuclear community to develop accurate and inexpensive neutron detection and spectroscopy techniques. The goal of this work was to focus on a detection medium that can effectively replace ^{3}He based neutron detectors, while also possessing properties that allow it to perform well as a neutron counter in a layered neutron spectrometer setup. ^{3}He has long been the material of choice for detecting neutrons, but high cost and limited supplies have created the impetus to find a replacement material. LiCAF (lithium calcium aluminum fluoride) is the material of choice for this work because of its desirable properties: non-hygroscopic, low γ sensitivity, available in larger sizes, transparent and high light yield [1,2]. ZnS: ^{6}LiF and ZnS: $^{10}B_2O_3$ are other alternatives that have been recently studied, and while ZnS has many desirable properties as a scintillator, there are also significant disadvantages including a long afterglow time (upwards of 100 μs) and opacity to its own light [3]. ^{10}B based neutron detectors have the advantage of a larger neutron interaction cross section, however, the reaction products are lower energy than ^{6}Li and include gammas [4].

LiCAF has been previously evaluated by Viererbl et al. and separately by the Pacific Northwest National Laboratory (PNNL) [1,2]. Viererbl et al. focused on the ability to discriminate signals from neutron and gamma radiation and PNNL evaluated LiCAF for application in a portal monitoring system. Using only pulse-height analysis, Viererbl et al. found that gamma radiation with energies above 1400 keV started to interfere with the neutron peak from a 0.5 cm thick wafer of Eu:LiCAF [2]. The discrimination capability, however, is highly dependent on the size and density of small grains (scintillator crystals) in the rubber, and also the geometry of the detector. PNNL found that the LiCAF neutron detector's sensitivity for a bare and moderated ^{252}Cf source is 1.01 ± 0.09 and 1.54 ± 0.23 cps/ng respectively with large rubberized Eu:LiCAF detectors measuring 100 cm long, 26 cm wide and 3 cm thick [1]. This is approximately 40%–60% of the value suggested as a requirement for portal monitors [5].

* Corresponding author.
E-mail address: michael.ford@afit.edu (M.A. Ford).

https://doi.org/10.1016/j.nima.2018.08.016
Received 18 June 2018; Received in revised form 19 July 2018; Accepted 6 August 2018
Available online 17 August 2018
0168-9002/Published by Elsevier B.V.

Wafers of rubberized Eu:LiCAF were obtained from Tokuyama Corporation, Japan. First, the wafers were evaluated for their neutron response and the ability to discriminate neutrons from gammas. Wavelength shifting fibers (WSF) from Kuraray (B-3) were embedded in the wafers to convert the scintillation photons to a frequency that is optimized for SensL C-Series blue-sensitive silicon photo-multipliers (SiPMs). SiPMs have been used for many years in applications ranging from medical imaging, 3D ranging and sensing, biophotonics, high energy physics, and now for threat identification [6–9]. The scintillation light of particle detectors has historically been collected with traditional photo-multiplier tubes. However, recent advances have significantly reduced the dark noise of SiPMs. Coupling the low dark noise with the greater transparency and relatively high light output of LiCAF creates ideal conditions to introduce SiPMs to inelastic neutron scattering detectors [10].

Previous work with LiCAF indicates that it has the ability to perform well as a neutron detector. The scintillation properties of LiCAF make it desirable for use with silicon photo-multipliers because of its high light output, excellent transparency, and ability to discriminate neutrons from gammas. Custom electronics were developed as part of this work to readout, amplify, filter, and count the neutron pulses created in LiCAF by a neutron flux. The methodology and results are discussed herein.

2. LiCAF scintillator

Two compositions of LiCAF are available from the Tokuyama Corporation. It is available doped with europium or cerium, has an effective Z of 15 and density of 2.99 g/cm^3 [11]. There are a few primary differences between the dopants that led to Eu:LiCAF being chosen for this work. The light yield of Eu:LiCAF is approximately eight times that of Ce:LiCAF. The decay constant of Ce:LiCAF is 40 ns, while it is >1 μs for Eu:LiCAF. This is a disadvantage of Eu:LiCAF, as the shorter decay constant is desirable, however, since the material was tested in environments with a relatively low neutron flux, the longer decay constant was not a significant issue. The luminescent wavelength of the Eu:LiCAF is 360–390 nm as compared to the Ce:LiCAF at 280–320 nm. The optimal wavelength for the Sensl-C series silicon photo-multiplier is the peak sensitivity region (approximately 425 nm) where the photon detection efficiency (PDE) is at 42% with an overvoltage of 5.0 V [12]. The photon detection efficiency is highly dependent on the overvoltage of the SiPMs. Finally, europium has a much larger neutron absorption cross section than cesium does, especially near the thermal energy region [13]. This is a disadvantage of the europium atoms, but it is not a serious issue because of the trace amounts of atoms that are present only in the Eu:LiCAF fibers embedded in the rubberized wafer; the primary interaction with the europium is (n, γ) and the gammas will not significantly interact with the low-Z material.

Eu:LiCAF/rubber (2×10^{21} ^{6}Li/cm^3) was used throughout this work. The neutron absorption percentage of the rubber-matrix LiCAF is approximately 5% higher than ^{3}He at 10 atm for 25 meV neutrons [11]. While the neutron absorption percentage is much larger for the pure LiCAF crystal, since it is largely dependent on the number of ^{6}Li atoms, the cost of the material is an order-of-magnitude higher. The neutron absorption percentage of pure cerium or europium doped LiCAF crystal is ~60% for a 1 mm thick sample (thermal neutrons), whereas it is only ~17% for the Eu:LiCAF/rubber used for this work. Thermal neutrons have a high cross section for absorption in ^{6}Li resulting in the following reaction:

$$^1_0\mathrm{n} + ^6_3\mathrm{Li} \longrightarrow ^3_1\mathrm{H}\ (2.73\ \mathrm{MeV}) + ^4_2\mathrm{He}\ (2.05\ \mathrm{MeV}). \quad (1)$$

Both the tritium and the alpha particles interact in the LiCAF crystal scintillator, emitting photons that are transported via the WSFs to the SiPMs, where a current is created. The current is then amplified and converted to a voltage signal, then filtered and converted to a digital signal using a comparator. The digital signals can then be counted/recorded using a field-programmable gate array (FPGA) or microcontroller.

A disadvantage of Eu:LiCAF is the relatively low α/β ratio. The difference between the ratio of absorbed energy and the light yield for the gamma radiation and heavy charged particles (HCP) is caused by the quenching dependence on the linear energy transfer (LET). The ratio for Eu:LiCAF is 0.2 [14]. This presents an issue for bulk Eu:LiCAF crystals, as the scintillation light from the high-energy HCPs is approximately equivalent to a 1 MeV gamma. The discrimination problem can be mitigated by controlling the geometry of the crystals since the range of the fast electrons induced by gamma rays is significantly longer than the HCP range. In the case of the rubberized LiCAF, controlling the size of the small LiCAF grains embedded in the rubber matrix is essential, and also the number and spacing of the small grains to optimize discrimination capability while not significantly sacrificing neutron detection efficiency. Using a smaller grain size of LiCAF in the rubber matrix is advantageous for discrimination purposes as it allows the fast electrons induced by gamma rays to easily escape the scintillator grain before depositing their full energy [15]. Another method of controlling the sensitivity to gammas is by reducing the overall LiCAF in the wafers (reducing the number of small grains). A drawback to the lower density of LiCAF is the reduced neutron detection efficiency.

Each wafer of rubberized Eu:LiCAF scintillator used throughout this work is 10 × 10 cm × 0.5 cm thick. There are also 30 WSF fibers embedded in both the X and Y axes through the wafer. The WSFs are desirable for signal readout because of the flexibility of the rubberized LiCAF and the custom geometries, which makes using traditional PMTs difficult to implement. However, the gammas and neutrons tend to interact with the WSFs (as they are very similar to plastic scintillation fibers) [15]. [15] found that the spectrum obtained from the WSFs without the Eu:LiCAF scintillator is almost the same as the one obtained with the Eu:LiCAF scintillator and the WSFs when using a ^{60}Co gamma source. The gamma/WSF signals are an undesirable side-effect of utilizing the wavelength-shifting fibers, however the scintillation pulses of the WSFs are on the order of nanoseconds, and an active low-pass filter will be utilized throughout this work to discriminate the gamma/WSF signals from the neutron pulses (~1 μs).

3. Electronics

Maintaining the portability of the detectors was a primary consideration in designing the electronics for the pulse counting and discrimination. Traditional PMTs were not used because of their size and power requirements; SiPMs offer similar specifications as PMTs without many of the disadvantages [6–9]. The advantage of using SiPMs is that they are extremely small, are insensitive to magnetic fields, operate ideally with relatively low voltage (30 V), and the output signal can be easily amplified and filtered with basic electronics. A disadvantage of SiPMs is that their detection efficiency and gain are highly dependent on temperature.

A schematic of the pulse counter circuit is shown in Fig. 1. The timing and gain of each component was carefully chosen to ensure that proper pulse-shape filtering and amplification can be achieved. The first essential component is the Sensl C-Series SiPM, which has a microcell size of 35 μm and a peak sensitivity of 425 nm. The stage 1 is a simple npn transistor used to buffer the current (unity gain) from the SiPMs and the stage 2 amplifier is an Analog Devices AD8007 (ultralow distortion high-speed amplifier, 650 MHz, 1000 V/μs slew rate) with a gain of +2. Initial testing was conducted with the SensL evaluation board (MicroFC-SMA-300xx-35u) to ensure that the light emitted from the LiCAF would result in a sufficiently high signal-to-noise ratio (SNR) after the inefficiencies from both the WSFs and the photon detection efficiency of the SiPMs (maximum of 42%). Fig. 2 shows the results from comparing the SensL evaluation board to the custom circuit using a BGO crystal and ^{68}Ge gamma source. A BGO scintillator was used for the early electronic testing because it has a well documented light output from the 511 keV annihilation gammas that could be used for comparison in simulations. The original signal from the evaluation board (green trace,

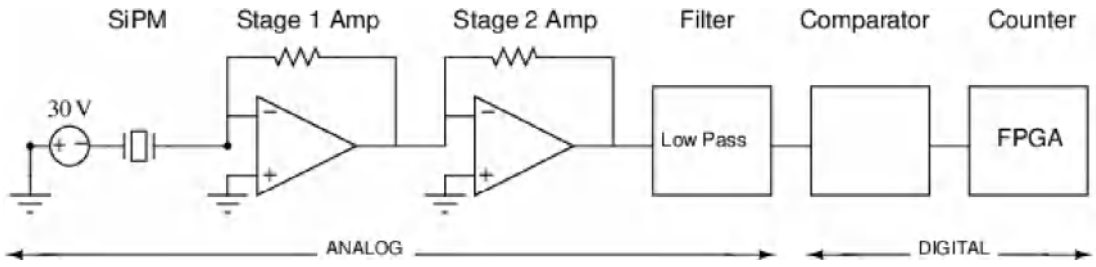

Fig. 1. Schematic showing the signal flow through the LiCAF pulse counter circuit.

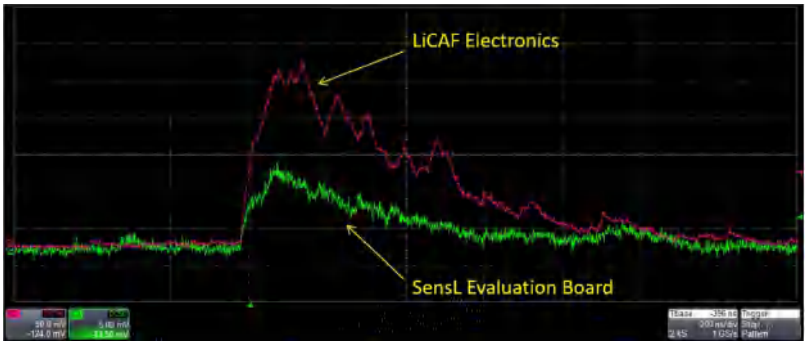

Fig. 2. Comparison of the output signals from BGO scintillator using the SensL evaluation board and the portable electronic readout employing the Analog Devices AD8007. (For interpretation of the references to color in this figure legend, the reader is referred to the web version of this article.)

5 mV/div) had a peak amplitude of about 10 mV, whereas the custom circuit using the AD8007 amplifier (red trace, 50 mV/div) had a peak amplitude of approximately 250 mV and a faster slew rate with the same BGO crystal.

The signal shown in Fig. 2 is collected at the output of the stage 2 amplifier; it then must go through a filter, comparator, and finally a counter. The purpose of the filter after the amplifiers was to suppress the faster pulses in the rubberized Eu:LiCAF wafer and WSFs. The gamma/WSF pulses have a higher frequency than the neutrons, thus filtering the faster pulses, in conjunction with pulse-height discrimination, allowed most of the gamma/WSF pulses to be rejected. An active low-pass filter was developed using the Analog Devices ADA4857-1 Operational Amplifier. This amplifier was chosen because of its desirable properties: ultralow distortion, low power, low noise, and high speed. The next step after the filter was to perform pulse-height discrimination. This was done with the Maxim Integrated MAX995, high speed, low voltage comparator. The comparator outputs a digital pulse anytime the user-defined threshold was exceeded. Using a micro-controller or field programmable gate array, the rising edges of the comparator output can be counted to determine the number of neutrons that interacted with the LiCAF. The comparator was setup in burst guard mode, which limits pulse pile-up. Counts were only recorded when the pulse signal amplitude exceeded the user-defined threshold.

Modeling of the circuit was performed using LTSpice, and the circuit was validated using a BGO crystal with a ^{68}Ge source. BGO has a lower light output and slower decay time than other available crystals (such as LYSO), which would more accurately reflect the properties of LiCAF. While LiCAF does emit approximately 40,000 photons per neutron [16], many of the photons are not collected in the fibers, or are lost in the transmission process. Fig. 3 shows the persistent oscilloscope traces of the output of the stage 2 amplifier (left column of scope image), and the right column of the scope image shows the comparator output due to the gamma interaction in the BGO. The digital output of Fig. 3 (right) is not in persistence mode and only shows a pulse each time the comparator threshold voltage is exceeded. The LTSpice simulation of the circuit matched in amplitude, pulse shape, and rise time with the experimental results.

4. Experiment

A sample 10 × 10 cm wafer of rubberized Eu:LiCAF was evaluated. The wafer was 0.5 cm thick and had WSF (polystylene matrix and organic phosphor) embedded along both the X and Y-axes. There were 30 one mm diameter fibers embedded on each axis (Fig. 4) to allow for position-dependent readout, and to provide a sufficient number of photons reaching the SiPMs. It is generally accepted that only about 1% of the wavelength shifted photons will reach the SiPMs after accounting for the collection efficiency and re-emission of photons along the axial direction of the fibers [10]. A light-tight box was placed around the entire wafer/electronics assembly to minimize the number of ambient photons interacting with the SiPMs, which served to keep the signal-to-noise ratio as large as possible. To further reduce the number of ambient photons that have the potential to decrease the SNR, caps were 3-D printed out of a black nylon (PA 11) to fit tightly over the SiPM, while only having one extrusion at the top to allow the fiber to fit tightly (Fig. 5). The 3-D cap was also used as a way to mount and hold the fiber in place while the optical glue dried (Loctite 349). The electronics used to amplify the SiPM signal required +/−5 V, ground, negative high voltage (approximately 30 V [12]), and a variable reference voltage for the comparator. The output of the electronics was either an SMA cable or a single wire for the digital pulse, depending on the analysis being performed. The SMA cable allowed output of the waveforms for post-processing, or the digital pulses can be used if neutron counts are the only interest.

Although the rubberized Eu:LiCAF has very low sensitivity to gammas, gamma interactions do occur. Because of the fast-signal suppression of the WSF scintillation events, the relatively small LiCAF grain size and density, and the fact that the neutrons deposit more energy in the scintillator (from the high energy and low range of the alpha particle and triton), the two sources can be very effectively distinguished using the combination of filtering and pulse-height discrimination.

Data was taken through two experiments: one at the Air Force Institute of Technology using an Adelphi Technology DD108 Neutron Generator. The DD108 produces ~2.45 MeV neutrons at a continuous emission rate of 1×10^9 n/s with 100 kV accelerating voltage, an operating beam current of 3 mA and deuterium flow rate of 8.0

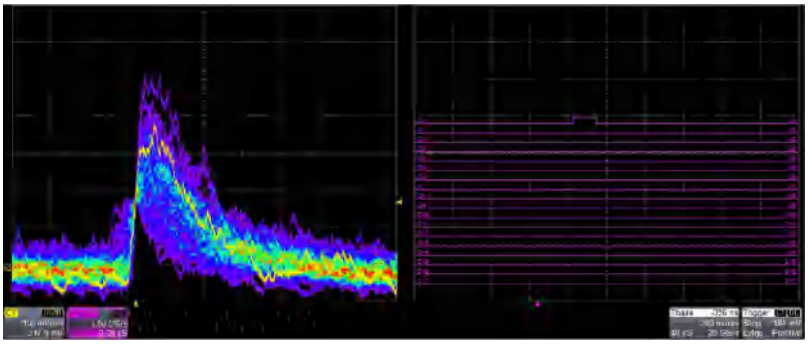

Fig. 3. Persistent oscilloscope traces of the electronic circuit mated to a 4 mm × 4 mm BGO crystal with a ^{68}Ge gamma source (left), and the output digital pulse from the MAX995 comparator (right). The digital output (right) is not in persistence mode and shows a digital pulse whenever the threshold voltage is exceeded.

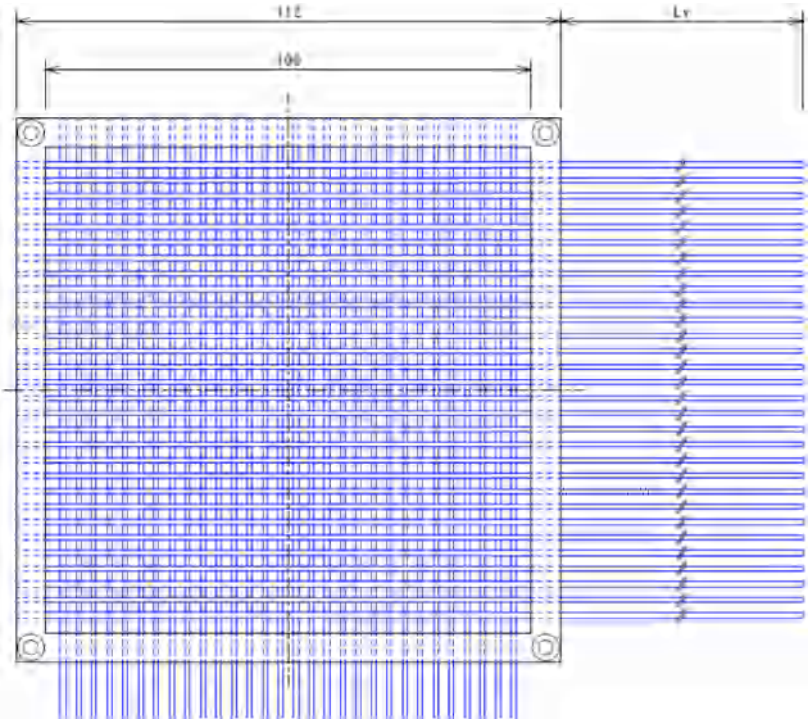

Fig. 4. CAD drawing of the LiCAF wafer from Tokuyama.

SCCM [17]. The second set of tests were conducted at the University of Michigan using a Thermo Scientific MP320 DD neutron generator with an emission rate of 1×10^6 n/s, and also a ^{252}Cf source with a calculated activity of 2.77×10^6 Bq [18]. For the neutron generators, a single LiCAF wafer was placed perpendicular to the isotropic flow of neutrons from the core of the generator at a distance of 20 cm. Testing with the ^{252}Cf source was conducted with the source 25 cm from the front face of the LiCAF wafer.

4.1. Pulse height discrimination

Initial testing with the rubberized Eu:LiCAF wafer concentrated on using pulse-height discrimination, in conjunction with pulse-shape filtering, to allow a simple neutron count output. Three sets of data were taken with a single WSF in the center of a LiCAF wafer. Background neutron counts were negligible. The first test collected 3000 digitized traces using a ^{137}Cs source placed directly adjacent to the wafer. Data was taken with an SMA cable output terminating into a Teledyne WaveRunner 620Zi oscilloscope. MATLAB was used for post-processing and the area under each of the pulses was integrated (integrated energy) and plotted. Integrated energy was used as a metric since the

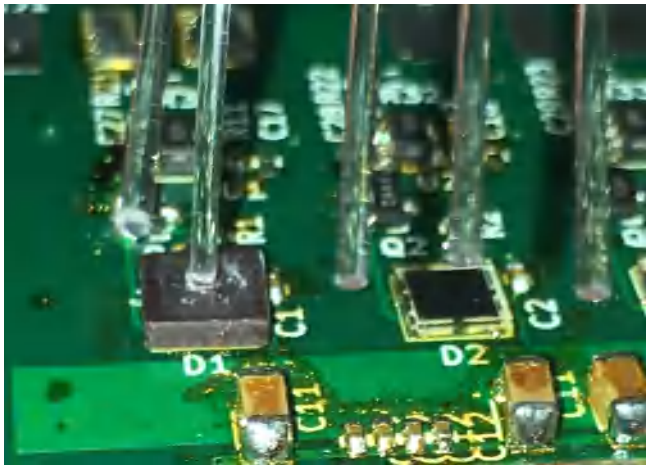

Fig. 5. Mating of the fibers to the SiPMs using 3-D printed caps and optical glue.

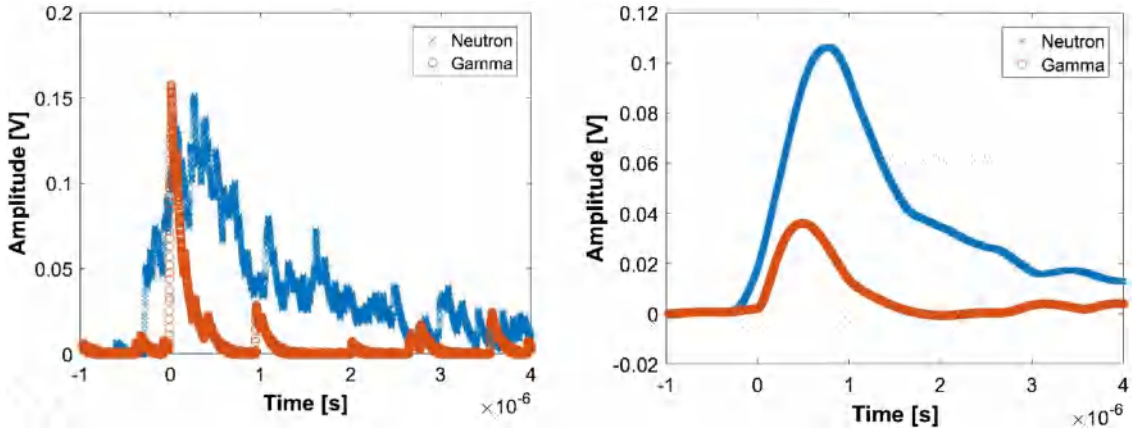

Fig. 6. Digitization of the gamma/WSF and neutron pulse before being filtered (left) and after a low-pass filter (right). In this case, the pre-filter pulse amplitude of the neutron is less than the pre-filter amplitude of the gamma/WSF. After filtering, pulse-height discrimination can be used to eliminate the gamma/WSF because of the fast-pulse suppression.

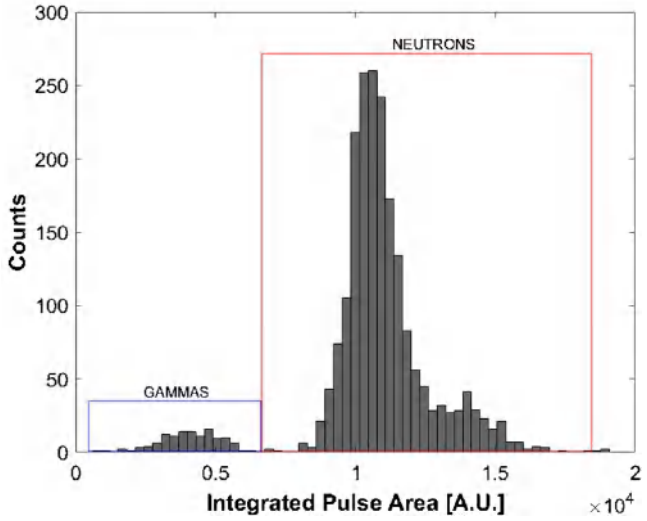

Fig. 7. The LiCAF detector is able to discriminate neutrons from gammas and WSF scintillation events using pulse-shape analysis followed by pulse-height discrimination. This is the result of capturing waveforms for a 5 min test run with both ^{137}Cs and the DD Generator.

current generated by the SiPM is proportional to the number of photons collected; integrating the area of the pulse gives a linear correlation to the energy deposited in the scintillator. The next test recorded 3000 traces again, this time using only the DD generator. Fig. 6 shows that the area of the neutron pulses is significantly larger than the area of the gamma/WSF pulses. From Fig. 6 (left), the original amplitude of the two pulses from the gamma/WSFs and neutrons are approximately the same amplitude (so close that pulse-height discrimination is impractical). However, after filtering the two pulses (an active low-pass filter with f_c = 360 kHz was used), the amplitude of the higher frequency gamma/WSF pulse is reduced to less than half the amplitude of the neutron pulse as shown in Fig. 6 (right). Pulse-height discrimination can now be applied and the gamma/WSF count rejected. The threshold value was experimentally adjusted with the LiCAF until the gamma/WSF counts were minimized without significantly affecting the number of neutron counts. For simplicity, the threshold value was decreased until the gamma/WSF counts were less than the square root of the neutron counts.

A final data set was collected for 5 min with both the ^{137}Cs and the DD generator, generating the results shown in Fig. 7. Because of the differences in timing properties of the gamma/WSFs and neutrons in the wafers, the high-energy reaction products of the neutron interaction

Table 1
Neutron/gamma discrimination performance using comparator threshold of 70 mV.

Test	cps
Background	<0.01
^{137}Cs	0.103
DD Generator	10.7
DD Generator + ^{137}Cs	10.7

with ^{6}Li, and the low LiCAF density in the rubberized matrix, good discrimination can be accomplished. The lower energy counts (left peak of Fig. 7) are the faster pulses from the gammas/WSFs and the peak on the right is the result of the larger, slower neutron pulses. The peak on the right side of Fig. 7 has a total of 3204 counts, whereas the peak on the left has 63. The total counts for both gamma/WSFs and neutrons is 3267, and this is the value that would be used for "neutron counts" in a spectroscopy application. When setting a pulse-height threshold, it is not practical to raise the threshold so high as to eliminate all of the gamma/WSF counts, instead, the goal is to raise it high enough as to keep the gamma/WSF counts at or below the square root of the total counts (below counting statistics). For this test, the reported counts is 3267 ± 58 neutrons, which is approximately consistent with the number of hits in the right peak of Fig. 7. A 70 mV threshold value was set to maintain the gamma/WSF counts below the error of the neutron counts for the collection time and activity of sources used. An overview of the testing results is shown in Table 1. The results show that there is negligible addition to the neutron counts with the addition of the ^{137}Cs source.

The comparator's threshold voltage was set with an HP 3245A precision voltage supply. The electronics have the ability to output the pulse waveform via an SMA cable, however, once the threshold value is determined it is no longer necessary to use the waveform output. The comparator will output a CMOS pulse anytime the threshold voltage is exceeded. For use in spectroscopy, only the digital output would be necessary and any pulse counter could be employed to tally the number of neutrons captured in the LiCAF.

4.2. Pulse-shape analysis

The focus of testing at the University of Michigan was to determine the rubberized Eu:LiCAF wafer's ability to discriminate neutrons from gammas and WSF scintillation events using only pulse-shape analysis. Pulse-shape analysis was applied to separate gammas and WSF scintillation events from neutron waveforms based on the traditional charge integration method. The peak of each waveform was found, and an integration window on each side of the peak was selected to find the area of the peak down to a user-specified threshold level. A Figure

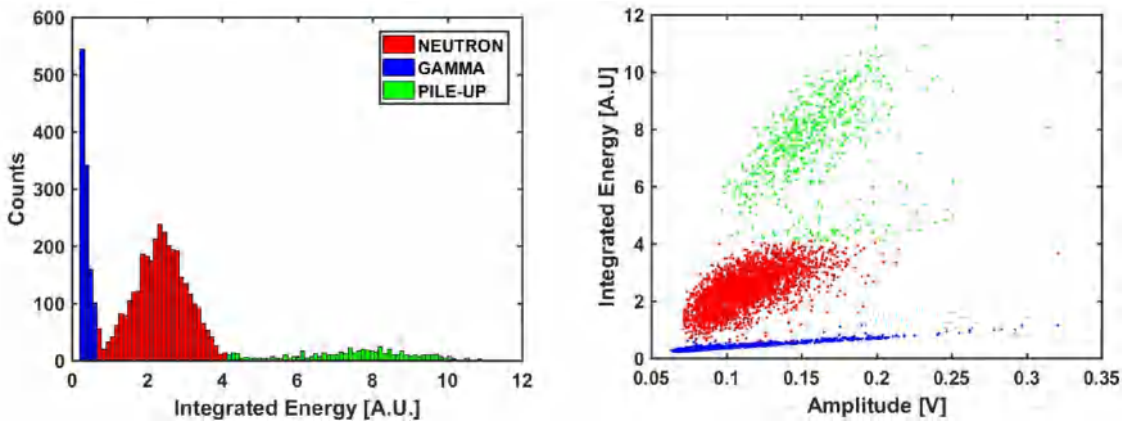

Fig. 8. Histogram showing the integrated energy of each waveform from a one-hour DD neutron generator run at the University of Michigan (left). Scatter plot showing integrated area versus pulse-height of each waveform from the one-hour DD neutron generator run (right). Regardless of the gamma/WSF pulse-height, the faster rising edge and lower integrated area of the gamma/WSF event allows the neutrons to be easily discriminated from the gammas. (For interpretation of the references to color in this figure legend, the reader is referred to the web version of this article.)

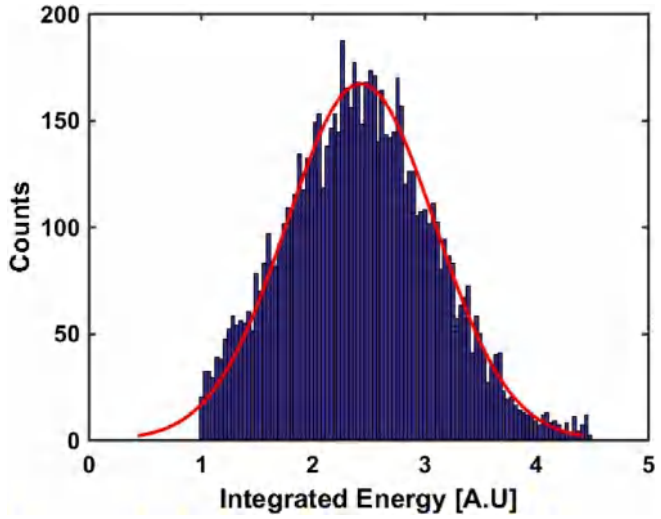

Fig. 9. When the neutron pulses are separated from the gamma/WSF pulses in Fig. 8 (left), the histogram can be fitted to a Gaussian curve allowing extraction of μ_n and σ_n to determine the FoM.

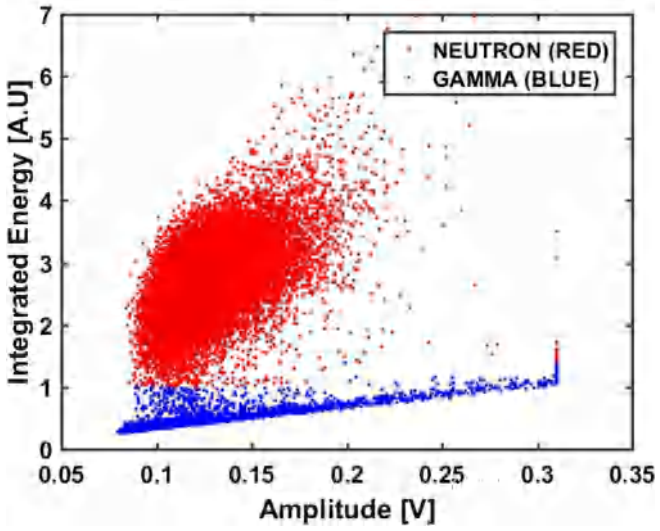

Fig. 10. Scatter plot showing integrated area versus pulse-height of each waveform from a 15 h data collection period with a ^{252}Cf source.

of Merit (FoM) was utilized to evaluate the ability of the rubberized Eu:LiCAF wafer to discriminate the neutrons from the gammas and WSF scintillation events. The FoM was defined as:

$$\text{FoM} = \frac{d}{FWHM_n + FWHM_\gamma} \tag{2}$$

where d is the distance between the centroids (μ_n–μ_γ) of the gamma and neutron peaks when the integrated energy of the waveforms are plotted on the same axis via a histogram, and the $FWHM_n$ and $FWHM_\gamma$ are the full width half-maximum (2.35σ) of the neutron and gamma peaks of the histogram, determined by approximating each peak with a Gaussian fit.

A one-hour DD neutron generator run was first conducted to evaluate the effectiveness of pulse-shape analysis with the rubberized Eu:LiCAF. A LiCAF wafer was placed adjacent to the target plane of the generator with 2.5 cm of HDPE placed between the LiCAF wafer and the generator tube. The waveforms were digitized with a Hantek 6074BE PC oscilloscope and post-processing was accomplished using MATLAB. The resulting histogram is shown in Fig. 8 (left). There are three visible peaks in the histogram. The leftmost peak (blue) is a result of the gammas striking the LiCAF crystal or WSFs and causing scintillation photons to be emitted, or fast-electron interactions in the WSFs. The central peak (red) is a result of neutron (and a few gamma) interactions in the LiCAF. The tail of the neutron pulses is, on average, much longer than the tail of the gamma/WSFs resulting in a larger area. Finally, the rightmost peak (green) is a result of pulse pile-up in the LiCAF and is indicative of deadtime in the electronics. To compute the FoM, the peaks were separated into respective histograms for neutrons and gammas (Fig. 9 shows the neutron histogram). After fitting the histograms with Gaussian curves, the FoM can be calculated. An overview of the fitting parameters is shown in Table 2.

Table 2
Specifications of discrimination and Gaussian fit parameters.

Property	DD	^{252}Cf
Baseline discrimination level	10 mV	10 mV
μ_n	2.433	2.678
μ_γ	0.410	0.507
σ_n	0.664	0.610
σ_γ	0.169	0.182
FoM	1.033	1.167

The gamma histogram is partially skewed at lower energies. This is a result of the discrimination method that was used to calculate the integrated energy. With a low-level discrimination, there is a

minimum area that will be represented and this feature is evident in the histogram. Using the parameters from the Gaussian fits, the FoM of the discrimination was calculated to be 1.03 for the DD generator. Plotting the integrated energy versus the pulse-height represents the capability of pulse-shape analysis using rubberized Eu:LiCAF. Fig. 8 (right) shows a clear distinction between the gamma/WSF waveforms (bottom), the neutron waveforms (middle) and the pile-up waveforms (top). Table 2 also shows data from the ^{252}Cf source. The FoM of the ^{252}Cf is better than the DD generator because of the lower average energy neutrons and longer data collection time. It is also worthy to note that the scatter plot for the ^{252}Cf (Fig. 10) does not have the "pile up" region that is evident in Fig. 8 (right) from the DD generator.

For neutron spectroscopy applications, this analysis shows that pulse-shape analysis is possible, however, a disadvantage of using the analysis is that it requires digitization and/or integration of each waveform to determine if the pulse was a result of a neutron or gamma/WSF interaction. Because each layer of rubberized Eu:LiCAF has 60 optical fibers for signal read-out, the amount of instrumentation required to analyze each waveform and perform live pulse-shape analysis is difficult in practice, hence pulse-height discrimination may be the preferred method in a layered spectrometer system.

5. Conclusions

LiCAF shows potential to replace ^{3}He in many neutron detection applications. While a pure LiCAF crystal was not evaluated here, the scintillation photons are easily detectable in the rubberized form with commercial off-the-shelf (COTS) SiPMs. In addition, discrimination between neutrons and gammas can be performed using simple and compact electronics which would enable highly mobile applications. LiCAF shows promise using both pulse-height discrimination and pulse-shape analysis. Pulse-height discrimination allowed for a simple neutron-count output where the gamma counts were below the neutron counting statistics, and a FoM of 1.03 was demonstrated using pulse-shape analysis with the DD neutron generator. The FoM with a ^{252}Cf source was calculated to be 1.17.

One of the key considerations with using SiPMs is the SNR. Often times, the small signal of SiPMs can get lost in high noise environments, whether from photon noise from improper shielding of the SiPMs or electronic noise induced in the circuit. Care must be taken to properly amplify the current pulse of the SiPM (done herein with a transimpedance amplifier), then filter the resulting voltage signal. A threshold applied to the pulse height then allows for pulse-height discrimination, and digital pulses can then be counted, and recorded as neutron "hits". The flexible shape of rubberized LiCAF and the use of compact SiPMs instead of traditional, bulkier PMTs allows for the creation of custom, palm-sized neutron spectrometers requiring no more than a single battery to power. Future testing with LiCAF will include assembly of a ten-layer spectrometer utilizing pulse-height discrimination to count neutrons and the incident neutron energy will be determined via spectrum unfolding. Additional testing will be done with only the polystylene matrix and organic phosphor WSFs to evaluate how they react as stand-alone scintillation detectors.

Acknowledgments

This work was supported at the Air Force Institute of Technology by the Defense Threat Reduction Agency, United States (HDTRA17-245-26). Views expressed in this paper are those of the authors and do not necessarily reflect the official policy or position of the Air Force, the Department of Defense, or the United States Government.

References

[1] M. Woodring, R. Kouzes, M. Demboski, R. Cameron, J. Magana, Characterization of the Tokuyama Corporation LiCAF Neutron Detector, Tech. Rep., Pacific Northwest National Laboratory, 2015, p. 21, PNNL-ACT-10032.

[2] L. Viererbl, V. Klupák, M. Vinš, M. Koleška, J. Šoltés, A. Yoshikawa, M. Nikl, LiCaAlF 6 scintillators in neutron and gamma radiation fields, Int. J. Modern Phys. Conf. Ser. 44 (2016) 1660234, http://dx.doi.org/10.1142/S2010194516602349.

[3] T. Nakamura, M. Katagiri, N. Tsutsui, K. Toh, N.J. Rhodes, E.M. Schooneveld, H. Ooguri, Y. Noguchi, K. Sakasai, K. Soyama, Development of a ZnS/10B2O3 scintillator with low-afterglow phosphor, J. Phys. Conf. Ser. 528 (1) (2014) http://dx.doi.org/10.1088/1742-6596/528/1/012043.

[4] F.D. Amaro, C.M.B. Monteiro, J.M.F. dos Santos, A. Antognini, Novel concept for neutron detection: proportional counter filled with 10B nanoparticle aerosol, Sci. Rep. 7 (1) (2017) 41699, http://dx.doi.org/10.1038/srep41699.

[5] R.T. Kouzes, J.H. Ely, A.T. Lintereur, E.K. MacE, D.L. Stephens, M.L. Woodring, Neutron detection gamma ray sensitivity criteria, Nucl. Instrum. Methods Phys. Res. A 654 (1) (2011) 412–416, http://dx.doi.org/10.1016/j.nima.2011.07.030.

[6] M. Foster, D. Ramsden, A compact neutron detector based on the use of a SiPM detector, in: IEEE Nuclear Science Symposium Conference Record, 2008, pp. 1882–1886. http://dx.doi.org/10.1109/NSSMIC.2008.4774758.

[7] J.B. Mosset, A. Stoykov, U. Greuter, M. Hildebrandt, N. Schlumpf, H. Van Swygenhoven, Evaluation of two thermal neutron detection units consisting of ZnS/ 6LiF scintillating layers with embedded WLS fibers read out with a SiPM, Nucl. Instrum. Methods Phys. Res. A 764 (2014) http://dx.doi.org/10.1016/j.nima.2014.07.060.

[8] A. Stoykov, J.B. Mosset, U. Greuter, M. Hildebrandt, N. Schlumpf, A SiPM-based ZnS:$ˆ6$LiF scintillation neutron detector, 2014, arXiv:1408.6119, http://dx.doi.org/10.1016/j.nima.2015.01.076.

[9] S. Gnecchi, C. Jackson, *A1×16* SiPM array for automotive 3D imaging lidar systems, Int. Image Sensor Soc. (2017) 133–136.

[10] N. Rhodes, Scintillation detectors, Neutron News (23) (2012) 26.

[11] K. Fukuda, Scintillators Developed by Tokuyama for Neutron Detection Functional Fluoride Group, Tech. Rep., Tokuyama Corporation, 2014.

[12] SensL, C-Series Low Noise , Fast , Blue-Sensitive Silicon Photomultipliers, Tech. Rep., SensL Corporation, 2014, pp. 1–17.

[13] IAEA, ENDF - Europium Neutron Total Cross Section. URL https://www-nds.iaea.org/exfor/servlet/E4sSearch2.

[14] D. Sugimoto, K. Watanabe, K. Hirota, A. Yamazaki, A. Uritani, T. Iguchi, K. Fukuda, S. Ishidu, N. Kawaguchi, T. Yanagida, Y. Fujimoto, A. Yoshikawa, H. Hasemi, K. Kino, Y. Kiyanagi, Neutron TOF experiments using transparent rubber sheet type neutron detector with dispersed small pieces of LiCaAlF6 scintillator, Phys. Proc. 60 (2014) 349–355, http://dx.doi.org/10.1016/J.PHPRO.2014.11.047.

[15] K. Watanabe, T. Yamazaki, D. Sugimoto, A. Yamazaki, A. Uritani, T. Iguchi, K. Fukuda, S. Ishidu, T. Yanagida, Y. Fujimoto, Wavelength-shifting fiber signal read-out from Transparent RUbber SheeT (TRUST) type LiCaAlF6 neutron scintillator, Nucl. Instrum. Methods Phys. Res. A 784 (2015) 260–263, http://dx.doi.org/10.1016/J.NIMA.2014.11.109.

[16] T. Yanagida, A. Yamaji, N. Kawaguchi, Y. Fujimoto, K. Fukuda, S. Kurosawa, A. Yamazaki, K. Watanabe, Y. Futami, Y. Yokota, A. Uritani, T. Iguchi, A. Yoshikawa, M. Nikl, Europium and sodium codoped LiCaAlF$_{6}$ scintillator for neutron detection, Appl. Phys. Express 4 (10) (2011) 106401, http://dx.doi.org/10.1143/APEX.4.106401.

[17] Adelphi, DD108 Neutron Generator Adelphi Technology, URL http://www.adelphitech.com/products/dd108.html.

[18] Thermo Scientific, Thermo Scientific MP 320 Lightweight, Portable Neutron Generator Thermo Scientific MP 320 Neutron Generator. URL https://assets.thermofisher.com/TFS-Assets/CAD/Specification-Sheets/D10497{~}.pdf.